ISSN 1573-160X, *PHYSICAL OCEANOGRAPHY*, Vol. 31, Iss. 4, pp. 486-506 (2024)
Original Russian Text © Yu. N. Goryachkin, D. I. Lazorenko, V. V. Fomin, 2024,
published in *Morskoy Gidrofizicheskiy Zhurnal*, 2024, Vol. 40, Iss. 4, pp. 534–555

Original article

Dynamics of Accumulative Coast under the Influence of Transverse Hydraulic Structure

Yu. N. Goryachkin, D. I. Lazorenko ✉, V. V. Fomin

Marine Hydrophysical Institute of RAS, Sevastopol, Russian Federation
✉ *d.lazorenko.dntmm@gmail.com*

Abstract
Purpose. The study is purposed at determining modern dynamics of the Lake Sasyk bay-bar (Crimean Peninsula) and the impact of the local seawater intake upon the coastal zone based on long-term *in situ* observations, satellite data and mathematical modeling. The study was conducted in view of the proposed construction of transverse hydraulic structures.
Methods and Results. Regular (2007–2014) and occasional *in situ* observations of the coastline dynamics at the Lake Sasyk bay-bar were used. The maximum inter-annual oscillations in the coastline locations are shown to be 5.8 m in the sections to the southeast from the transverse structure (seawater intake) and 3.4–7.2 m – in the sections to the northwest. Seasonal variability is significantly higher: the maximum range is 14.6 m in the sections to the southeast, and in those to the northwest – 26.7 m. The wave climate was investigated. The wave reanalysis data for 1979–2022 have shown that the southwestern direction of waves approaching the coast with a frequency exceeding 30% is most probable. The highest waves also come from this direction. The extreme values of wave characteristics which can occur once in *n* years were obtained. The mean long-term values of storm numbers in the area under study are given depending on their duration. Application of the *GenCade* integrated lithodynamic model permitted to obtain the estimates of changes in the coastline position in this area on the interannual scales.
Conclusions. The model calculations made it possible to reproduce the main features and trends in changes of the beach width in the area of the structure obtained due to *in situ* observations. The mean annual sediment flows in the area under study are directed clockwise (to the southeast) that is conditioned by the coastline orientation and the wave climate features. Difference between the mean annual sediment rates at the area boundaries is negligible – less than 4% of the multi-year average. This fact indicates insignificant impact of the structure upon the sediment total transfer to the southeast.

Keywords: Black Sea, Lake Sasyk, bay-bar, water intake, lithodynamics, mathematical modeling, wave climate, GenCade

Acknowledgments: the study was carried out within the framework of the theme of state assignment of FSBSI FRC MHI FNNN 2024-0016.

For citation: Goryachkin, Yu.N., Lazorenko, D.I. and Fomin, V.V., 2024. Dynamics of Accumulative Coast under the Influence of Transverse Hydraulic Structure. *Physical Oceanography*, 31(4), pp. 486-506.

Introduction

The largest accumulative formation of the coastal zone in Western Crimea – the Lake Sasyk bay-bar (Fig. 1) – is located between Yevpatoria and Saki. A motorway and a railway as well as other communications are laid along it. A complex of multi-storey hotels was planned to be built on the bay-bar in the early 2000s. The project included the construction of a number of transverse hydraulic structures (yacht marinas, berths, groins), but no detailed project development was

carried out. The completion of Simferopol – Yevpatoria – Mirny highway construction is scheduled for 2024. This project envisages the transfer of the highway from the Lake Sasyk bay-bar to bypass it. The administrative bodies of the Republic of Crimea announced the upcoming implementation of the project for the construction of recreational facilities on the bay-bar. The construction of transverse hydraulic structures is also involved. At the same time, recent negative experience of constructing such facilities during the implementation of embankment construction project on Lake Sakskoye bay-bar led to the need to revise the project, delay its implementation and unjustified financial costs [1]. In this regard, it seems relevant to study the coastal zone reaction to the construction of a transverse hydraulic structure for a specific area.

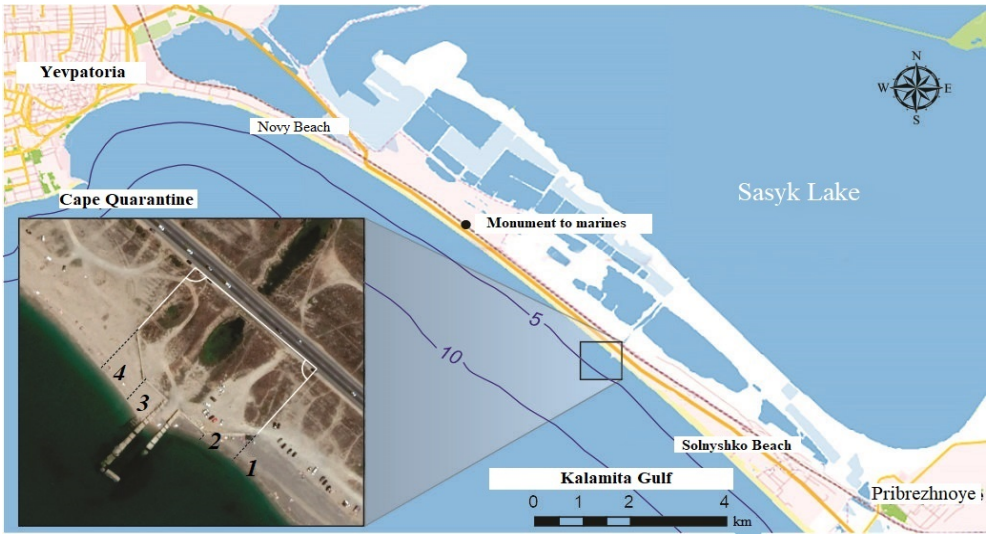

F i g. 1. Schematic map of the Kalamitsky Bay northern part. Inset shows a satellite image of seawater intake on the Lake Sasyk bay-bar, numerals denote section locations and numbers

This work is purposed at determining modern dynamics of the Lake Sasyk bay-bar and the impact of the local sea water intake upon the coastal zone based on long-term *in situ* observations, satellite data and mathematical modeling.

The most detailed studies of the Lake Sasyk bay-bar were carried out in 1930–1934 by an expedition led by Academician N.S. Kurnakov and Professor A.I. Dzens-Litovsky [1]. These studies were carried out in order to provide chemical industry with brine raw materials from the Crimean salt lakes. A bay-bar description based on the results of these works is given in [1], [2], [3].

[1] Dzens-Litovski, A.I., 1938. “Peresyps” (Bars) and “Limans” (Estuaries) of the Azof-Black Sea Coast and the Steppe Crimea. *Priroda*, (6), pp. 22-36 (in Russian).

[2] Dzens-Litovski, A.I., 1934. [Complex Hydrogeological Study of Salt and Mud Lakes and Estuaries]. In: Central Geological, Hydrogeodetic and Geodetic Department, 1934. [*The Water Resources of the Subsoil of the Earth at the Service of Socialist Construction. Issue 5: Mineral Waters*]. Leningrad, pp. 159-196 (in Russian).

[3] Kurnakov, N.S., Kuznetsov, V.G., Dzens-Litovski, A.I. and Ravich, M.I., 1936. [*Salt Lakes of Crimea*]. Moscow; Leningrad: Izd-vo AN SSSR, 278 p. (in Russian).

In [4], according to the data from the expeditions of the 1940s and 1950s, some considerations about the bay-bar origin are given. In the 1980s and 1990s, occasional observations were carried out by I.I. Mechnikov Odessa National University during summer student practical trainings; the information they obtained is summarized in [2].

Observations of aeolian processes were previously conducted at the bay-bar as well [3, 4]. Individual episodic observations of the bay-bar dynamics were carried out by various organizations in Crimea. However, the results obtained have not been previously published, but it was reported that there were no signs of significant changes in the coastline over the past 70 years as a whole, as indicated by the analysis of aerial and satellite images as well as contact measurement data [5].

Dynamics of the Lake Sasyk bay-bar according to contact and satellite data

The bay-bar stretches from the eastern border of Yevpatoria to the watershed between Lake Sakskoye and Lake Sasyk for 13 km. The maximum width is noted in the eastern part of the bay-bar (up to 800 m), the minimum – in the western one (150-200 m). The typical height above sea level is 1.5-2.3 m. The Lake Sasyk bay-bar is composed of sand, shell, gravel and pebbles. Some shell is mixed with sand in the largest fractions. The percentage of gravel and pebble fraction increases at the water edge, as we move south. The bay-bar formation is associated with a sea level rise during the Holocene, its age is, apparently, ~5000 years [6]. The mouths of several gullies and dry rivers formed a sea bay on the site of modern Lake Sasyk as a result of transgression. Subsequently, sediments that were formed southwards of the region under consideration during abrasion and solid runoff from rivers were included in the alongshore transport regime which led to the bay-bar creation.

The Lake Sasyk bay-bar is one of the main discharge points for alongshore sediment flows coming from the south. According to Yu.D. Shuisky, the main amount of sediment falls to the depths due to the relatively steep underwater slope (0.020), some of which, affected by wind, become a part of sandy kuchugurs (hills of aeolian origin), and the shells are worn away by up to 10% per year. He also considers that an average amount of 65 thousand m^3/year of sediments enters the discharge area of the Kalamitsky stream over a long-term period. At the same time, the flow capacity is not enough to accumulate them – on the contrary, a coastline retreat is observed [2]. Nonetheless, he shows the Lake Sasyk bay-bar growing by 1 m/year on the map in his work [5]. However, this contradicts reality, since with such an increase in the coastline during the period he indicates, the beach would have increased by one and a half times, and the pile piers that were on the bay-bar in the 1960s–1980s would have ceased to exist.

[4] Zenkovich, V.P., 1958. *Morphology and Dynamics of the Soviet Black Sea Coast. Vol. 1*. Moscow: AS USSR Publ., 187 p. (in Russian).

[5] Shuisky, Yu.D. and Vykhovanets, G.D., 2006. Map of Average Abrasion and Accumulation Rate. 1960-1994. In: L. I. Mitin, ed., 2006. *Atlas of the Black Sea and Sea of Asov Nature Protection*. St. Petersburg: GUNiO MO of the Russian Federation, 44 p. (in Russian).

The longest monthly observations of the coastline position were carried out in the 1980s by the Regime and Operational Station of Yevpatoria. Observations were performed in the western part of the bay-bar (the monument to marines) and in its eastern part (Solnyshko beach). According to these data, the maximum range of interannual fluctuations in the coastline position was up to 6 m, in the western part 2 m on average, in the eastern one – 4 m (Fig. 2). No significant trend is distinguished in the western part, in the eastern it is 0.7 m/year. However, the observation period is too short to consider this trend significant.

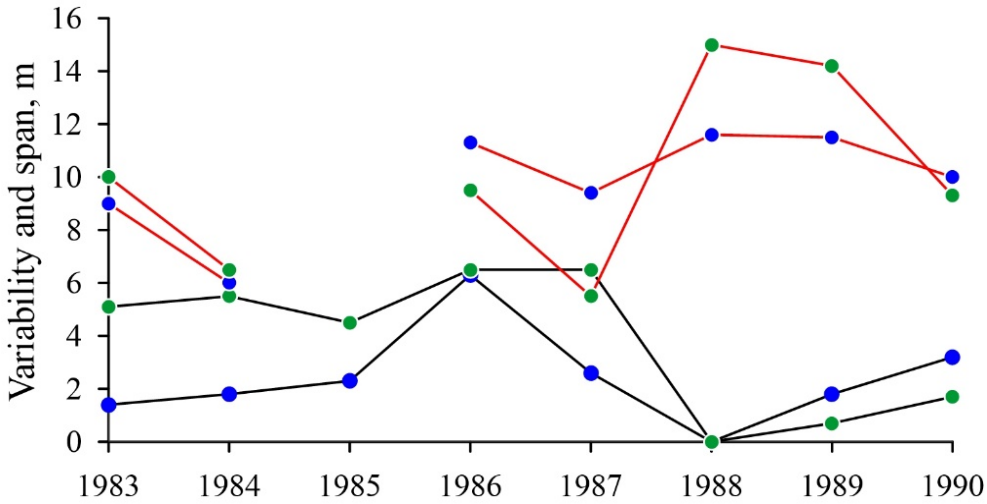

F i g. 2. Interannual variability of the coastline position (black curves) and the range of its seasonal fluctuations (red curves). Blue points show the western part of the Lake Sasyk bay-bar, green ones – its eastern part

The coast retreat by 6 m on both sections in 1986–1988 is noteworthy. It is possible that this is due to the construction of a transverse structure (NITKA facility) in 1983 in the area of Lake Kyzyl-Yar (located 12 km to the southeast) [5].

This object blocked the alongshore sediment flow directed counterclockwise in the Kalamitsky Bay. For this cause, the coastline of the Lake Sakskoye bay-bar located southwestwards retreated abruptly during 1984–1985 by 10 m [1]. Intra-annual fluctuations in the shoreline position are generally significantly greater than inter-annual ones and amount to 6–15 m (Fig. 2). In general, the maximum of the coastline progradation, according to these data, is typical for spring and retreat is typical for autumn.

After a break in the 1990s, observations were resumed in the 2000s.

In the period 2000–2014 (with short breaks), measurements were taken on a monthly basis at three sections in the bay-bar western part (Novy beach and the monument to marines). Additionally, measurements were taken in summer at three more sections of the bay-bar eastern part. Analysis of these data revealed that no significant trends in the coastline position changes were identified during this

period. The amplitudes of seasonal and interannual changes in the coastline position are within the limits characteristic of the period 1983–1990.

The data obtained at four sections in the water intake area in the bay-bar central part (2006–2014) are of the greatest interest. The seawater intake for salt extraction by *Solprom* Enterprise was built in the mid-1960s in the central part of the Lake Sasyk bay-bar. This transverse U-shaped reinforced concrete structure is 68 m long and has a depth of 3 m at the sea edge. It has not been used for its intended purpose since the 1990s and is in a dilapidated state (Fig. 3).

F i g. 3. Sea water intake on the Lake Sasyk bay-bar (view from the north)

The sections were located in pairs on the western and eastern sides of the water intake (Fig. 1, inset). Measurements were usually taken in the middle of each month. Since the distance between sections in a pair was 30 m, it is advisable to consider the coastline position variations as an average for two sections.

No statistically significant trends are distinguished in the interannual variability. The maximum range of interannual fluctuations is 5.8 m at sections *1*, *2* and 7.2 m at sections *3*, *4*. Seasonal variability is significantly higher: thus, their maximum range is 14.6 m at sections *1*, *2* and 26.7 m at sections *3*, *4*. In other words, seasonal variability range is three times greater than interannual variability one which corresponds to the values given above for the coast without hydraulic structures. At the same time, the range of fluctuations is approximately twice as large.

The pronounced antiphase of fluctuations is noteworthy. The coastline progradation westwards of the water intake corresponds to a retreat from the east and vice versa, while the correlation coefficient of the two series is 0.6. Obviously, this is due to variation in the direction of the alongshore sediment flow. This is even better seen in the graph of interannual variability obtained from the analysis of

satellite images from the Google Earth service. We used 19 images obtained during 2006–2022 (Fig. 4).

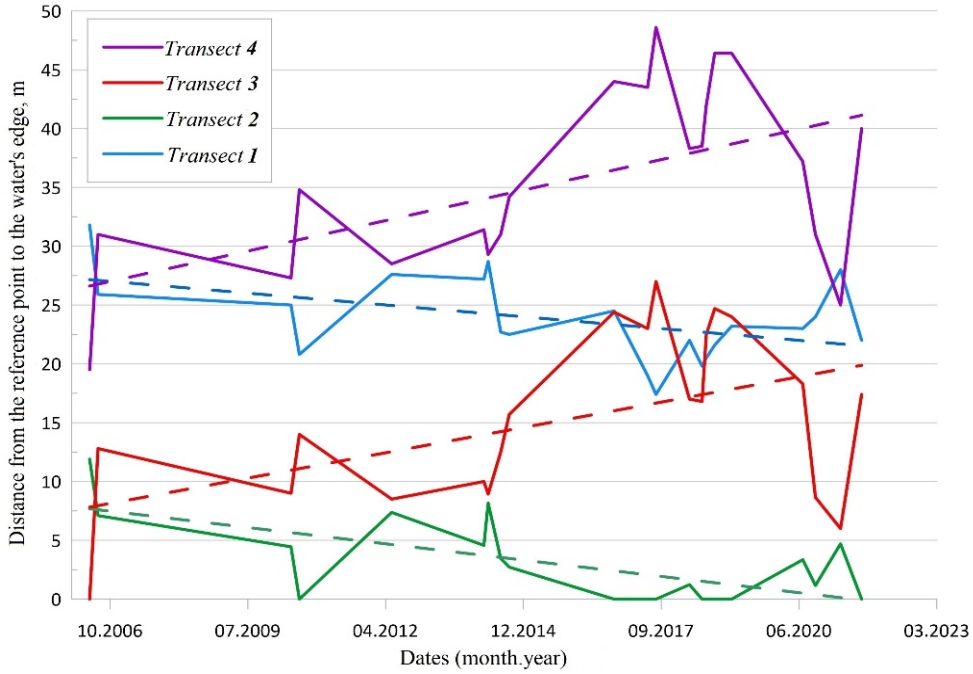

F i g. 4. Interannual variability of distance from the benchmarks to the water's edge at sections *1–4*

In addition to the antiphase of the coastline position fluctuations on both sides of the water intake, a positive trend is also noticeable on the western side and a negative one – on the eastern side.

To determine the coastline variability on the 500 meter long sections adjacent to the water intake on both sides, 50 cross-sections of the beach drawn every 20 m were analyzed. The main calculation algorithms described in the DSAS module [6] were applied for the analysis.

Fig. 5 shows the following results. For each section, the distances between the two lines corresponding to the maximum and minimum dates (resulting displacements) and the maximum coastline displacements (positive values of the range, independent of the date) were calculated. Fig. 5 also shows that the coastline advanced on the water intake western side by 8–20 m over a distance of 200–250 m and then insignificantly (1–3 m) over the period 2006–2022. On the eastern side, a coastline retreat is observed in all sections with a typical value of 4 m (maximum up to 8 m). At the same time, the maximum coastline displacements reach 26–28 m on the water intake western side and 12–16 m on the eastern side. Moreover, the greatest values are observed in five sections (100 m) on both sides of the water intake. The range of coastline fluctuations coincides almost completely

[6] Himmelstoss, E.A., Henderson, R.E., Farris, A.S., Kratzmann, M.G., Bartlett, M.K., Ergul, A., McAndrews, J., Cibaj, R., Zichichi, J.L. and Thieler, E.R., 2024. *Digital Shoreline Analysis System version 6.0: U.S. Geological Survey software release.* https://doi.org/10.5066/P13WIZ8M

with the values obtained during measurements at the sections. The comparison of figures can also show that it is necessary to use not the extreme dates of the images, but their entire available array to determine the coastline dynamics. To state the coastline interannual variability, the obtained values of the edge position for each section were averaged within a year and along the entire length of the sections. Undoubtedly, such averaging contains errors associated with the failure to take into account seasonal and spatial variability. Nevertheless, it gives some idea of the interannual variability (Fig. 6). The typical range of interannual fluctuations along the entire length of the sections is 1–7 m, which practically corresponds to the values obtained from measurements at the sections in 1983–1990. It should also be noted that the sediment accumulation predominantly on the western side of the water intake and the greater range of fluctuations compared to the eastern side can indirectly confirm our earlier conclusion about the predominance of a clockwise alongshore sediment flow in this area [7]. This differs from the opinions of other authors who believed that in the area under consideration the counterclockwise flow weakened gradually [4] [2].

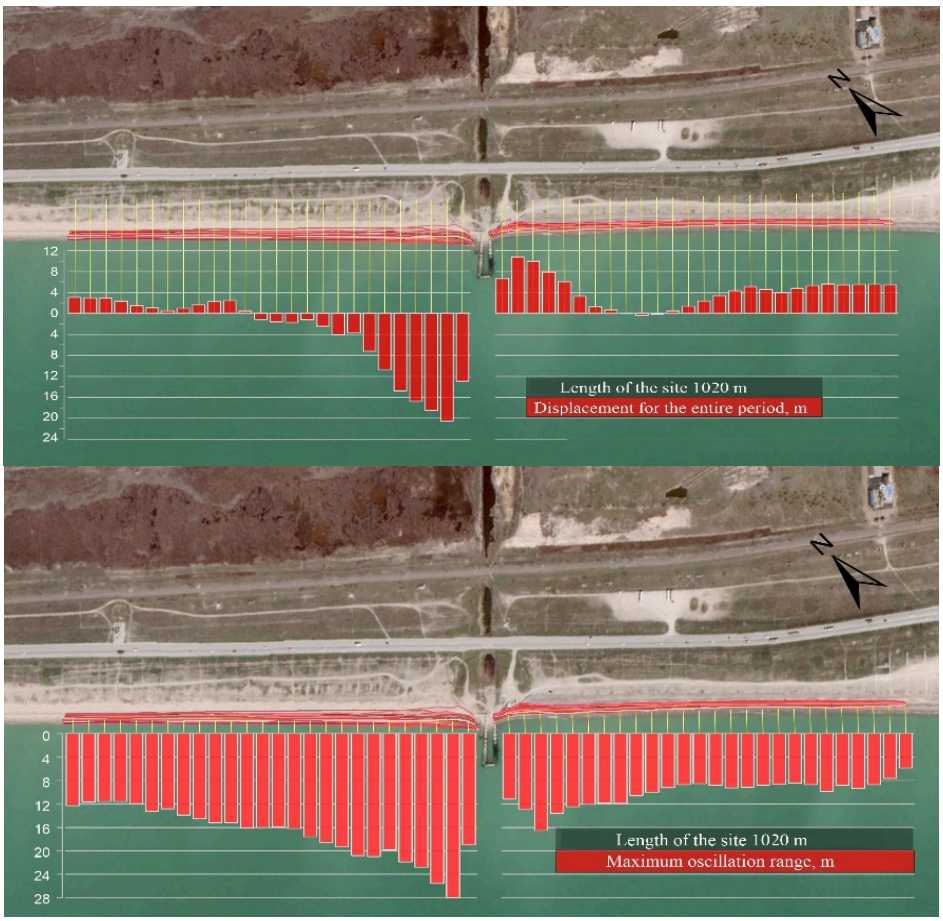

F i g. 5. Resultant (top) and maximum (bottom) coastline displacements in 2006–2022 based on satellite images

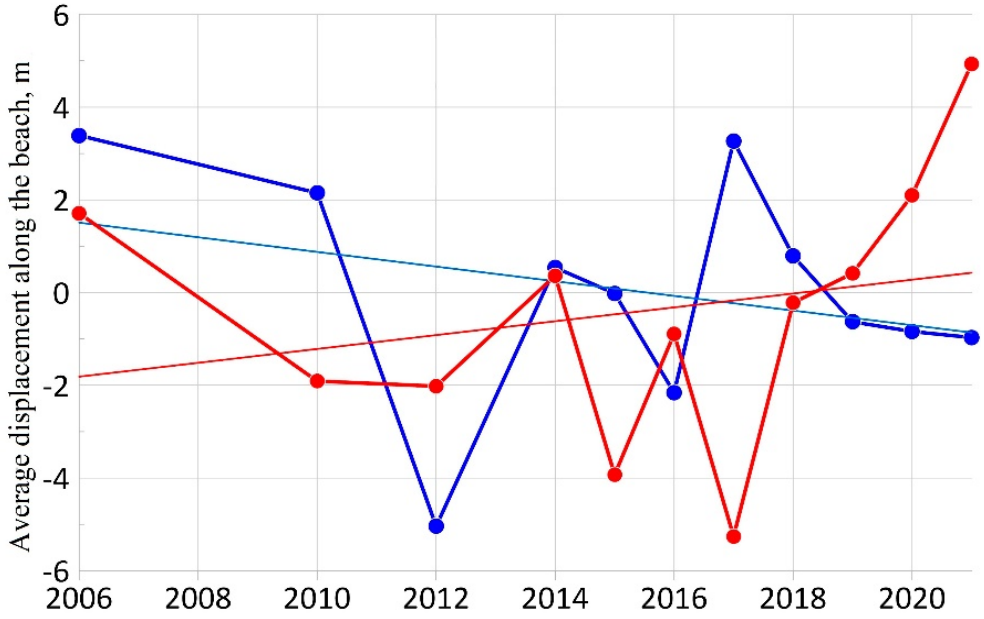

F i g. 6. Average over the section length interannual variability of coastline to the west (red curve) and east (blue curve) from water intake in 2006–2022. Straight lines show trends

Wave climate in the area of the Lake Sasyk bay-bar

The wave climate has a decisive effect on the lithodynamic processes in the area of the Lake Sasyk bay-bar. For its study, the data of wind wave reanalysis in the Black Sea for the period 1979–2022 (hereinafter referred to as the SWAN-ERA array) were applied. The array was obtained using SWAN [7] model on an unstructured computational mesh with thickening in the coastal zone [8]. ERA-Interim and ERA5 reanalysis data from the apps.ecmwf.int website were used as atmospheric forcing. The computational grid node closest to the technological structure with a depth of ~6.8 m was selected from SWAN-ERA array and long-term series including speed W and direction θ_a of wind, significant wave height h_S, mean wave period $\bar{\tau}$, mean wave direction θ were formed. The discreteness of series was 1 hour.

We are to consider some statistical characteristics of waves obtained from the calculated series. Fig. 7 demonstrates repeatability p of significant wave heights and mean wave periods. As can be seen, waves of 0.25 m height have the maximum repeatability. As the wave height increases, its repeatability decreases monotonically. Values h_S do not exceed 0.5 m in 71% of all cases. At $h_S \geq 1$, the waves have a repeatability of 12%, at $h_S \geq 2.0$ m – less than 1.5%. The highest repeatability of mean wave periods falls on the interval of 2.0–2.5 s which includes 56% of all cases.

[7] The SWAN Team, 2018. *SWAN User Manual. SWAN Cycle III Version 41.20.* Delft, Netherlands: Delft University of Technology, 121 p.

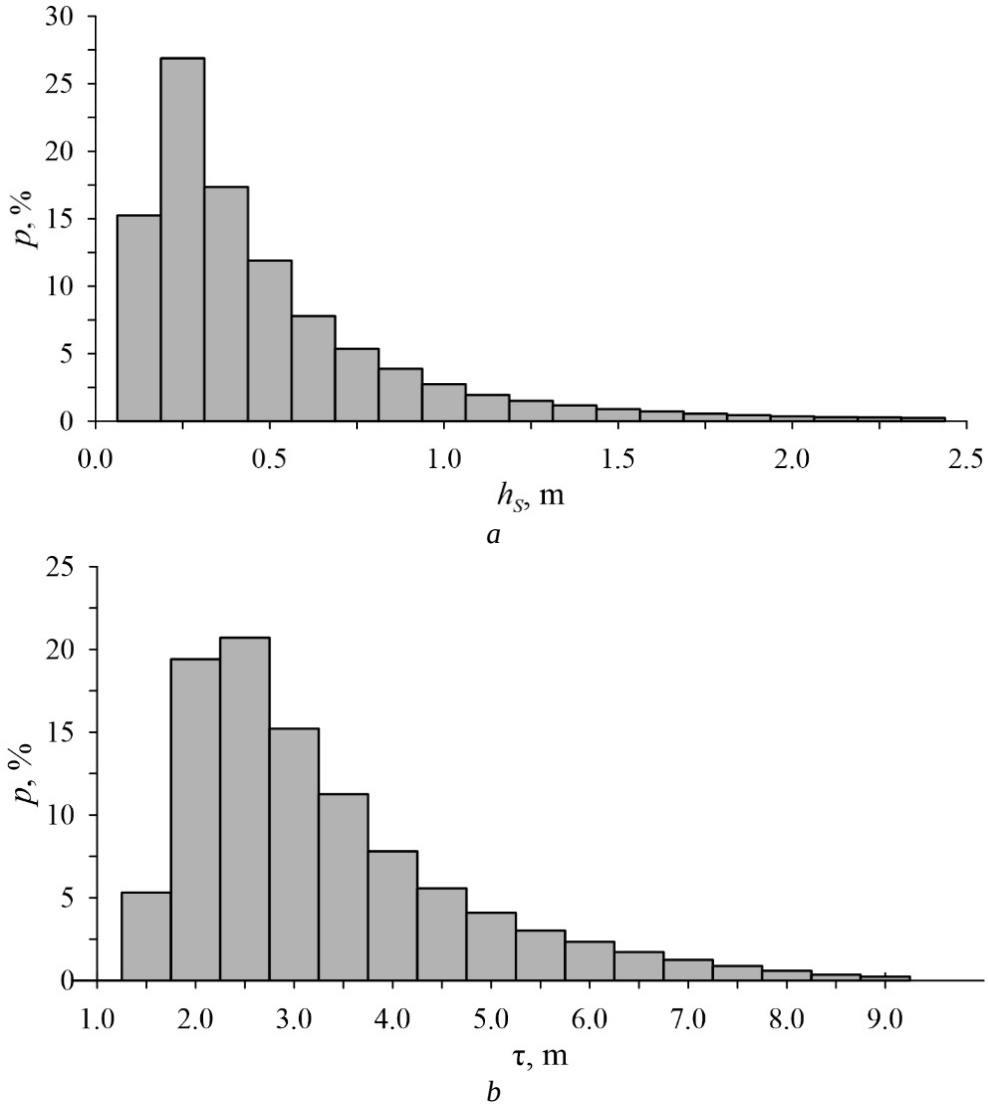

F i g. 7. Repeatability of significant wave heights (*a*) and wave mean periods (*b*)

Fig. 8 shows the wind speed repeatability by direction (wind rose). The northeasterly wind has the maximum repeatability (10%) and maximum speeds. From the sea, the southwesterly wind has the highest repeatability (6%). The most probable direction of wave approach to the shore is southwest with a repeatability of > 30% (Fig. 9). The highest waves (h_S > 2.5 m) also come from this direction. The maximum direction repeatability of waves approaching the shore correspond to the maximum repeatability of wind direction from the open sea. This approach of waves is facilitated by refraction, under the effect of which, as they approach the shore, the wave fronts are oriented parallel to the isobaths.

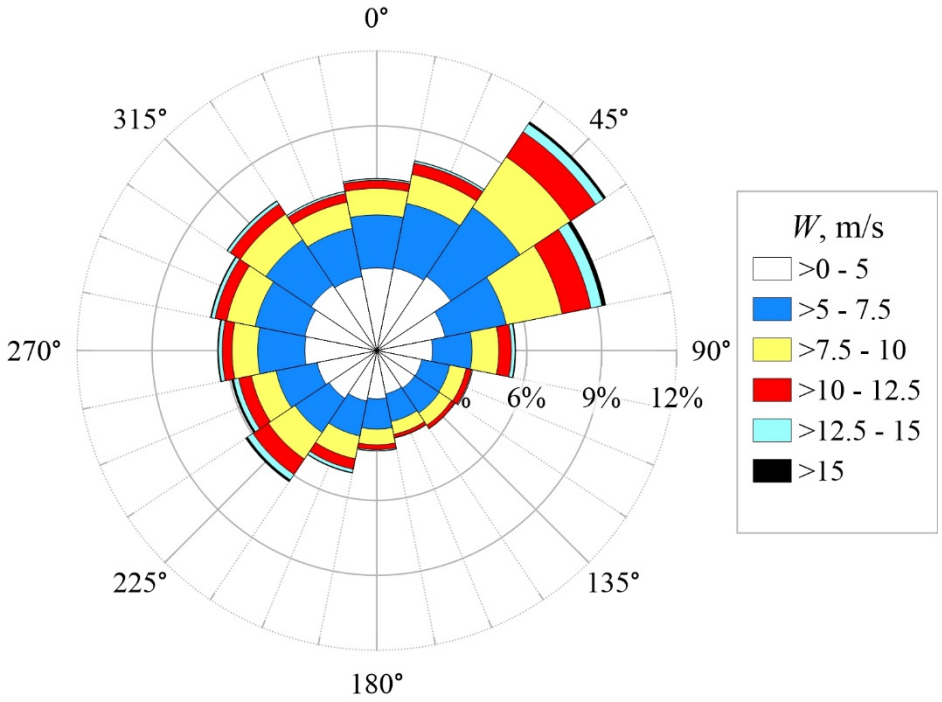

F i g. 8. Wind rose

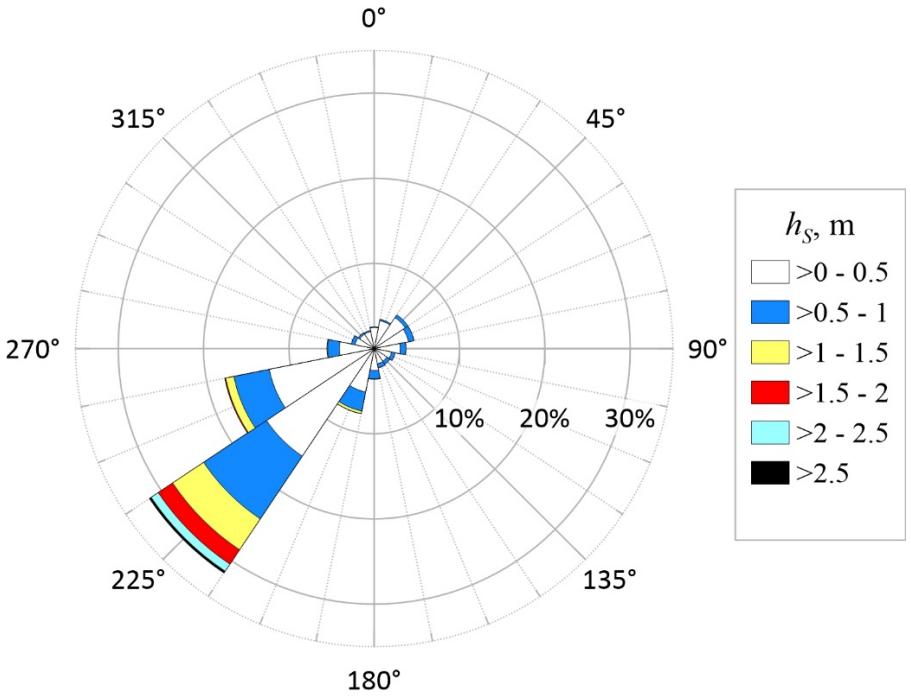

F i g. 9. Wave rose

Based on the available wave series, the duration of storm situations was also estimated. According to [1, 9], we applied the following condition as a criterion for identifying storm events

$$h_S \geq h_P, \tag{1}$$

where $h_P = \overline{h}_S + 2\sigma$ = 1.372 m is h_S threshold value; $\overline{h}_S$ = 0.544 m is h_S mean long-term value for a given series; σ = 0.414 m is h_S root-mean-square deviation from $\overline{h}_S$.

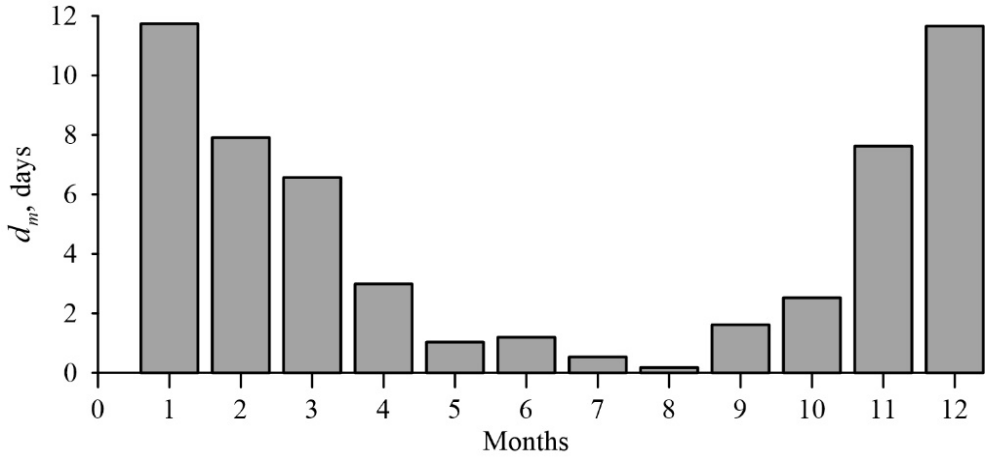

F i g. 10. Distribution of mean long-term duration d_m of storms by months

Fig. 10 demonstrates seasonal variation of mean annual duration d_m of storms. The longest storm situations in the area under study occur in December – January (d_m > 10), the minimum duration of storms (d_m < 1) is observed in July – August.

Fig. 11 represents the distribution of total duration d of storm situations by year. As can be seen, it varies within 4.9–26.0 days. The mean d value is 15.1 days. A long total duration of storms (d > 20 days) is observed in 1981, 1983, 1995, 2001, 2017 and 2021. The storms of 2001 and 2021 have the longest total duration.

Total distribution of storm duration does not provide an idea of their intensity. From this point of view, a more informative characteristic is the storm power index (*SPI*) [1, 9]:

$$SPI = h_d^2 \cdot T_d, \tag{2}$$

where T_d is storm duration (h); h_d is mean h_S(m) value over the storm period. In formula (2), when calculating T_d and h_d, all values of h_S series that satisfy condition (1) are summed up.

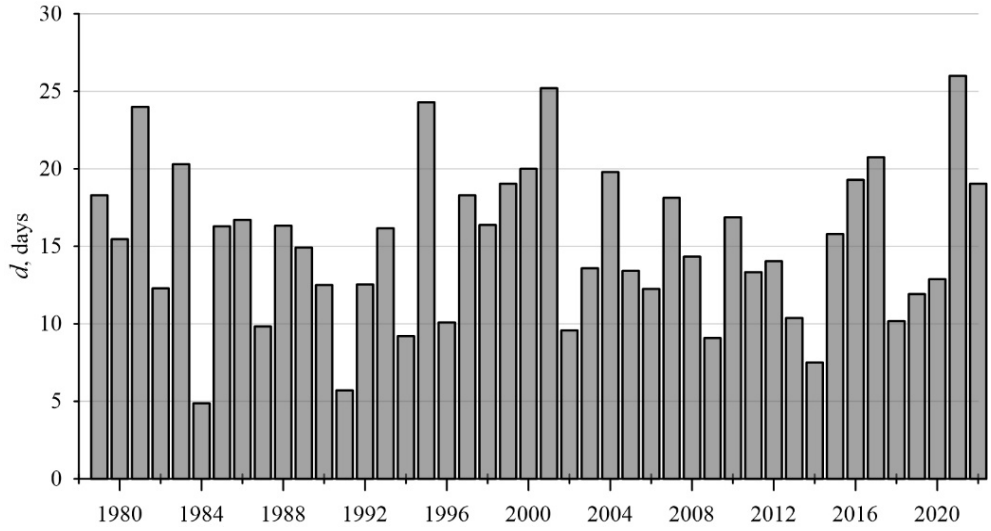

F i g. 11. Distribution of total storm duration *d* by years

Fig. 12 shows the distribution of total dimensionless storm power index $SPI_1 = SPI/SPI_0$ by year, where $SPI_0 = 0.573 \cdot 106$ m$^2 \cdot$h is the mean *SPI* value. 5 years (1994, 1995, 2001, 2009 and 2015) with increased storm activity ($SPI_1 > 1.5$) stand out in the graph. It is noteworthy that this list does not include 2021, which has the maximum total duration of storms (Fig. 11).

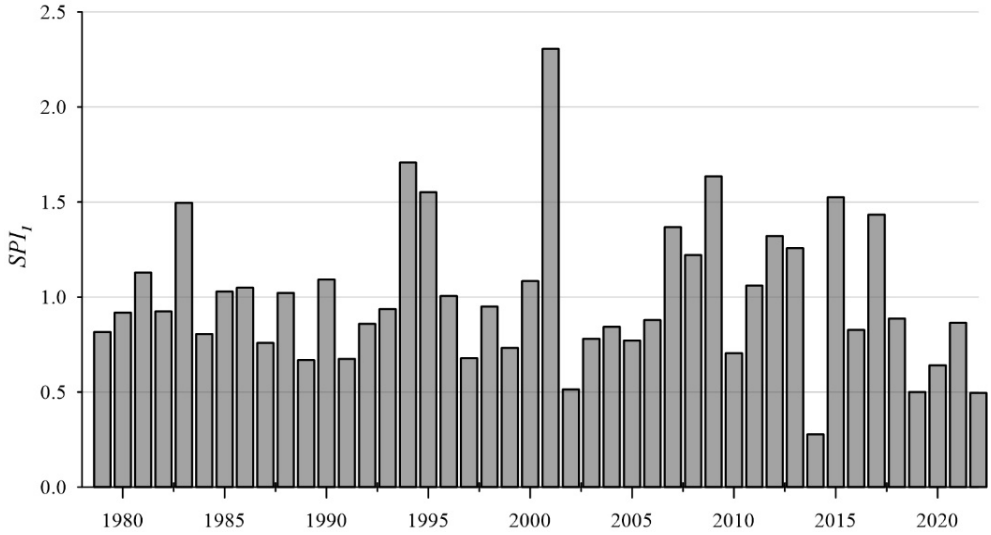

F i g. 12. Distribution of the storm power index SPI_1 by years

Extreme values of wave characteristics possible once per *n* years were estimated using the standard method described in [1]. Table 1 presents the estimates obtained. As can be seen, the wave heights of different probability and recurrence periods *T* differ slightly from each other which is due to the shallowness of the area under

study. With T increase from 1 to 100 years, h_S values increase by 19% and $h_{1\%}$ values – by 15%.

Table 1

Significant wave heights h_s, mean wave heights $\overline{h}$, wave heights of 13%-, 3%- and 1%-probability, mean wave periods $\overline{\tau}$, mean wave length $\overline{\lambda}$ in the system of storms which are possible once per 1, 5, 10, 25, 50 and 100 years

h_s, m	$\overline{h}$, m	$h_{13\%}$, m	$h_{3\%}$, m	$h_{1\%}$, m	$\overline{\tau}$, s	$\overline{\lambda}$, m
2.6	1.6	2.4	3.0	3.3	9.4	72
2.7	1.7	2.5	3.1	3.4	10.4	81
2.8	1.8	2.6	3.2	3.5	11.0	86
2.9	1.8	2.7	3.3	3.6	11.6	91
3.0	1.9	2.8	3.3	3.7	12.1	95
3.1	1.9	2.8	3.4	3.8	12.6	100

For a calculated storm that is possible once per 25 years, wave parameter values are as follows: h_S = 2.9 m, $h_{1\%}$ = 3.6 m, $\overline{\tau}$ = 11.6 s, $\overline{\lambda}$ = 91 m. Note that these wave characteristics are basic when designing coastal protection structures such as groins and breakwaters.

Table 2

Storm situation statistics for different gradations t_s

t_s, h	N_s	$\overline{T_d}$, h	SPI_m, m²·h
≥ 6	724	21	80
≥ 12	548	26	98
≥ 24	231	38	153
≥ 36	96	52	216
≥ 48	51	61	263

Now we are to analyze statistical characteristics of individual storms. For the sake of certainty, we consider storm situations with a duration (t_s) of at least 6 h. Table 2 provides the following for each of the five selected gradations t_s: total number of storms N_s; mean duration of storms $\overline{T_d}$; mean storm power index SPI_m. As the lower threshold of gradations increases, the number of storms decreases. If for gradation $t_s \geq 12$ h there are 548 storm events with mean

duration of 26 h and mean storm power index of 98 m^2·h, then for gradation $t_s \geq 48$ h only 51 events were identified. Mean duration of these events is 61 h and mean power index is 263 m^2·h.

Figure 13 shows the distribution of N_s values by years for five storm duration gradations t_s given in Table 2. The histograms shown there detail the information from Fig. 11. For all years except 2021, N_s value for $t_s \geq 6$ h is less than 25. According to $t_s \geq 6$ h gradation, 2021 has the largest storm number (N_s = 35). However, this year is inferior to other years in terms of the number of the longest (strongest) storms. For $t_s \geq 48$ h gradation, the number of storms in descending order is as follows: N_s = 6 for 1995; N_s = 5 for 1981; N_s = 4 for 2001; N_s = 3 for 1986 and 2007. Next comes a group of eight years with N_s = 2 which includes 2021. Another 12 years have N_s = 1. Mean long-term values of storm number by gradations of duration are as follows: 16 storms for $t_s \geq 6$ h; 12 storms for $t_s \geq 12$ h; 5 storms for $t_s \geq 24$ h; two storms for $t_s \geq 36$ h; one storm for $t_s \geq 48$ h.

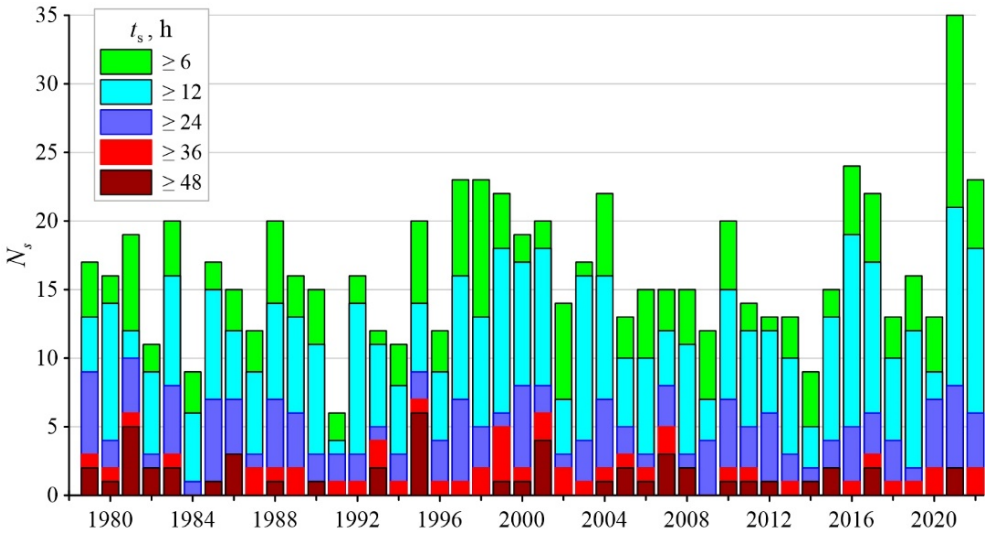

F i g. 13. Distribution of storm number N_s for different gradations t_s by years

Table 3 contains the characteristics of ten most powerful storms in the area under study based on wave reanalysis data for the period 1979–2022. Initial date of storm occurrence is given in the following format: year, month, day, hour. Four storms with *SPI* power index > 400 m^2·h are distinguished. The storms that began on December 25, 2000 and November 22, 2001 are the most powerful ones in the past 44 years.

T a b l e 3

Characteristics of extreme storms

Initial date	T_d, h	h_d, m	*SPI*, m²·h
2000122506	100	2.19	480
2001112210	118	2.01	476
2008112017	81	2.32	437
2015112009	75	2.37	423
1981120714	74	2.26	376
1995122303	67	2.26	344
2015013022	70	2.21	343
1979121019	65	2.27	334
1993012217	88	1.95	334
2021122409	57	2.39	325

Calculation of lithodynamic characteristics in the area of the Lake Sasyk bay-bar

Integral lithodynamic models [8], [9] are applied to assess long-term coastline variations [10, 11]. In this paper, we used *GenCade* [9] integral model to calculate the coastline variations in the area of the structure. It is based on the coastline evolution equation of the following form

$$\frac{\partial y}{\partial t} + \frac{1}{\left(D_B + D_C\right)} \frac{\partial Q}{\partial x} = 0. \tag{3}$$

Here, $y(x, t)$ is coastline coordinate, D_B is berm height, D_C is closure depth, $Q(x, t)$ is alongshore sediment flow. The x coordinate is defined in the interval $[0, L]$, where L is total length of the coastal zone section under consideration. A detailed description of the model is presented in 9 [11].

After integrating equation (3) over the variable x within the range 0–L, we obtain an ordinary differential equation

$$\frac{dV}{dt} = Q(0,t) - Q(L,t), \tag{4}$$

$$V = \left(D_B + D_C\right) \int_0^L y(x,t)dx, \tag{5}$$

[8] Hanson, H. and Kraus, N.C., 1989. *GENESIS: Generalized Model for Simulating Shoreline Change. Report 1: Technical Reference*. Washington: U.S. Army Corps of Engineers, 247 p. https://doi.org/10.5962/bhl.title.48202

[9] Frey, A.E., Connell, K.J., Hanson, H., Larson, M., Thomas, R.C., Munger, S. and Zundel, A., 2012. *GenCade Version 1 Model Theory and User's Guide: Final Report*. Vicksburg, MS: U.S. Army Engineer Research and Development Center, 187 p.

where V is total volume of sediments; $Q(0,t)$, $Q(L,t)$ are sediment flows on the left ($x = 0$) and right ($x = L$) computational domain boundaries, respectively. Equation (4) describes temporal variation of the total volume of sediments (formula (5)) at the studied beach area. If the right side of formula (4) is different from zero, then there will be an increase or decrease in the total volume of transported material.

The computational domain was a section of the coast totaling 1000 m selected in such a way that the structure was located in its middle. General direction of the coastline was 129° (the direction of the x-axis is close to northwest). Thus, positive Q values correspond to the movement of sediments from the southeast to the northwest in the adopted coordinate system. The calculation grid step in space was 20 m, the integration step in time was 4 min. According to [12], granulometric composition of bottom sediments at the water intake is characterized by the presence of a sand-gravel mixture, medium-grained and fine-grained sand. Moreover, the sand-gravel mixture is the predominant fraction. On this basis, the mean diameter of bottom sediment particles $d50$ was taken to be 0.8 mm.

To calculate the sediment flux Q in equation (3), a composite array of wave parameters (h_s, $\bar{\tau}$ and θ) obtained from *SWAN-ERA* data was applied. The array included only waves directed toward the shore, i.e. those waves for which the inequality $|\theta - \theta_N| < 90°$ is true, where $\theta_N = 219°$ is the direction of the normal to the general coastline direction of the area under consideration.

Based on preliminary calculations, the following values of model 9 parameters were selected: normalization constants in the formula for calculating the sediment flow $K_1 = K_2 = 0.77$; berm height $D_B = 2$ m; permeability coefficient of the structure $p = 0.2$. In all cases, closure depth in equation (3) $D_C = 5.5$ m. To estimate D_C, an empirical dependence of type 9 was applied:

$$D_C = 2.28 \cdot h_E - 68.5 \frac{h_E^2}{g\,\tau_E^2},$$

where h_E, τ_E are mean values of annual maxima h_s and $\bar{\tau}$, respectively, obtained from SWAN-ERA wave reanalysis data.

Calculations of the coastline variation in the technological structure area were carried out from March 12, 2014 to July 23, 2022, since, based on the analysis of Google Earth service satellite images, the greatest variability in the coastline position was observed during this period and the quality of images made it possible to digitize the coastline position. Numerical experiments revealed that the calculated coastline position corresponding to July 23, 2022 and its position in satellite images coincide in the best possible way with the selected values of model parameters. At the same time, a characteristic detail is traced: an accumulation of beach material takes place on the northwestern side of the structure, and coast erosion occurs on the southeastern side (Fig. 14).

In addition to coastline position variation, its increments were also calculated for each of four sections by formula $\Delta y^i(x) = y_f^i(x) - y_s(x)$, where $y_s^i(x)$ and $y_f^i(x)$ are coastline position at section i at the initial and final moments of time, respectively.

Positive Δy^i values correspond to the coastline progradation, negative values– to its retreat.

For each section *1–4*, the minimum values of calculated increments $\Delta y^i_{\min}$ were found and graphs of calculated relative increments $y_r^i(x) = \Delta y^i - \Delta y^i_{\min}$ were constructed for the simulated time period of March 12, 2014 – July 23, 2022 (Fig. 15). The trends (dashed lines of the same color) corresponding to relative increments for each section are also given in the figure.

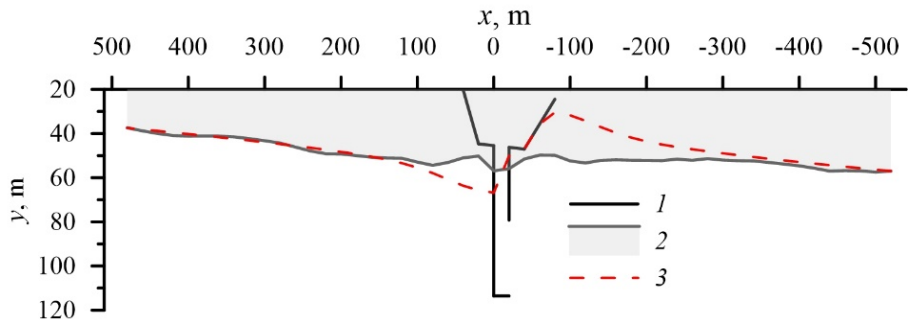

F i g. 14. Results of calculating the changes in coastline position: *1* – water intake construction; *2* – initial coastline position on March 12, 2014; *3* – calculated coastline position on July 23, 2022

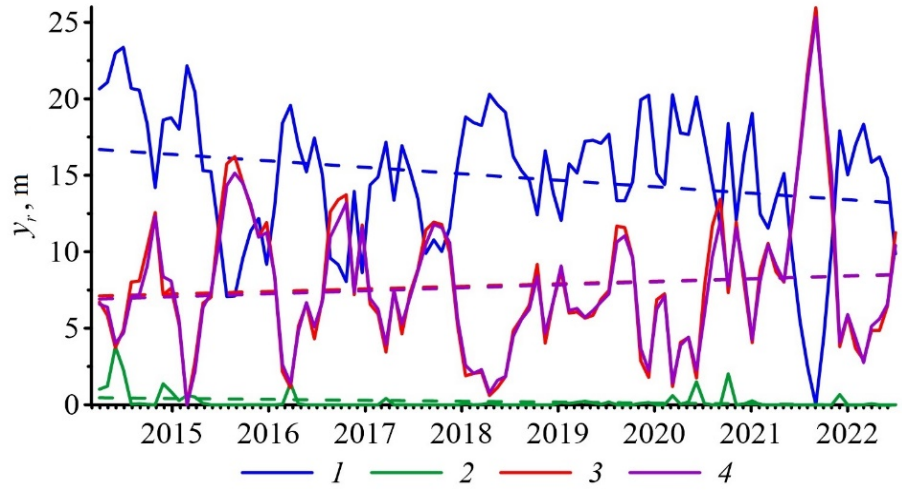

F i g. 15. Calculated relative increments of the coastline position y_r at sections *1–4* from 12.03.2014 to 23.07.2022. Dashed lines show trends

The calculation results revealed that there was a coastline retreat with mean long-term rate of ~ 0.42 and 0.06 m/year, respectively, at sections *1* and *2* and a beach width increase with a mean long-term rate of approximately 0.17 and 0.19 m/year took place at sections *3* and *4*. Thus, the model calculation results reproduce the effects of beach material accumulation northwestwards of the structure and coast erosion southeastwards of it, described above based on *in situ* data.

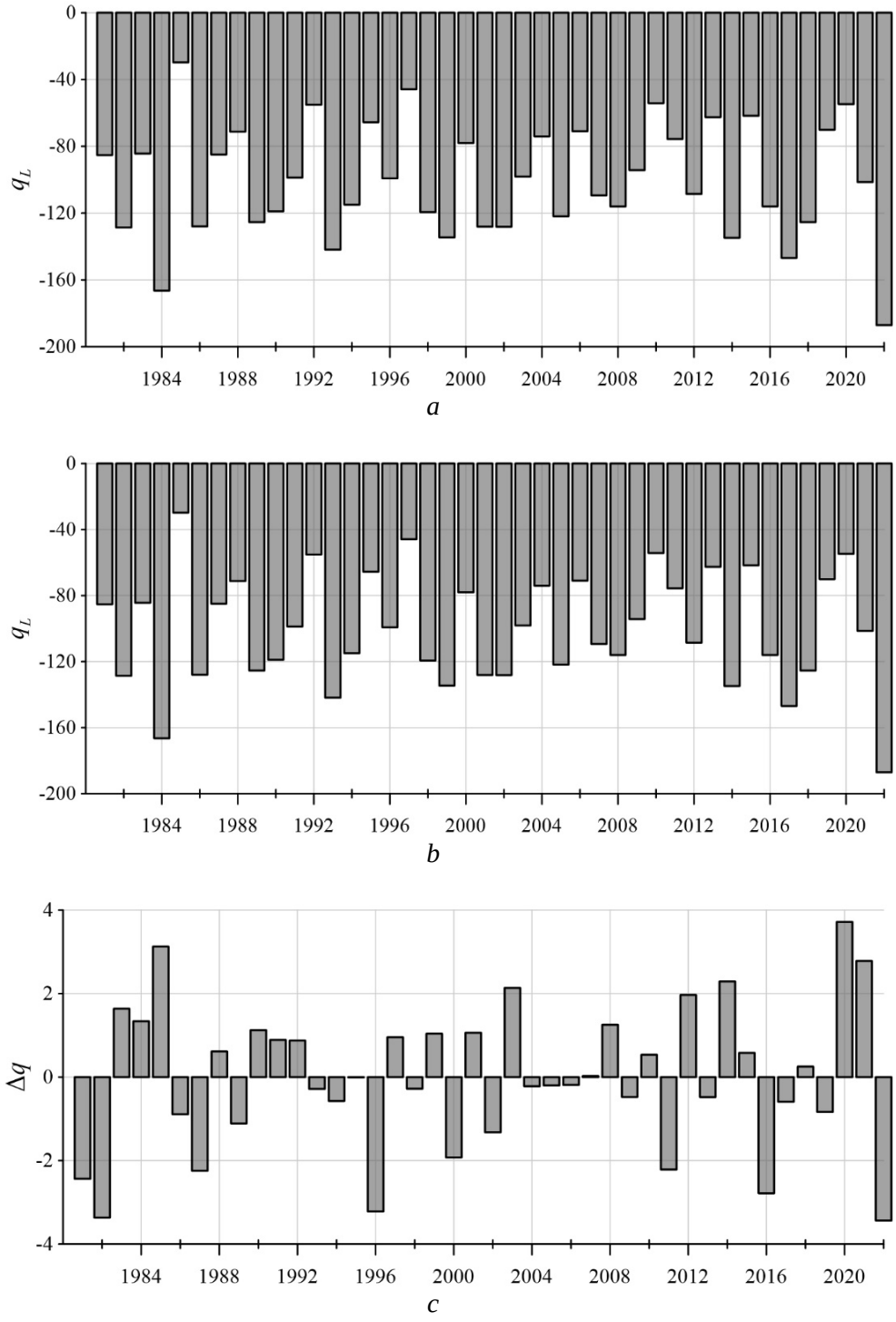

F i g. 16. Mean annual values of sediment rates: a – at the southeastern boundary ($x = 0$); *b* – at the northwestern boundary ($x = L$); *c* – difference between the sediment rates at the southeastern and northwestern boundaries

Mean annual values of sediment rates on the left (q_0) and right (q_L) computational domain boundaries, as well as their difference Δq, presented in dimensionless form are given in Fig. 16 for the period 1979–2022. They were calculated using formulas

$$q_0 = 10^2 \cdot \overline{Q_0}/q_m, \quad q_L = 10^2 \cdot \overline{Q_L}/q_m, \quad \Delta q = q_0 - q_L,$$

where $\overline{Q_0}$ and $\overline{Q_L}$ are mean annual sediment flows on the left and right boundaries, respectively; q_m = 75900 m^3/g is normalization constant representing mean long-term value of sediment flows at the left and right boundaries for 1979–2022 period.

As can be seen from the analysis of the presented diagrams, the mean annual values of q_0 and q_L are negative for the entire long-term time interval, i.e. the sediment flows are directed southeastwards. Their maximum absolute values reach $1.9 \cdot q_m$ and the standard deviation is ±35% of q_m. Unidirectionality of the flows is due to the coastline orientation and wave climate characteristics. In the area under study, the prevailing direction for the waves approaching the coast is sector $225° \le \theta \le 235°$ (Fig. 9), and the normal to the coastline general direction is oriented at an angle of θ_N = 219°. It is with this ratio of the angles between the waves approaching the coast and the normal to the coastline that the sediment flows of the southeastern direction will prevail.

The difference in flows at the Δq area boundaries changes sign from year to year (Fig. 16, *c*). According to equation (4), at $\Delta q > 0$, material accumulates in the area under study, at $\Delta q < 0$ material is consumed. As can be seen, the difference in flows between the left and right boundaries of the computational area is insignificant (less than ±4% of q_m). This indicates that the studied area is mainly transit of material. At the same time, local changes in the sediment flow near the technological structure do not have a significant effect on the total transport of bottom material in the southeastern direction.

Conclusion

A comprehensive study of lithodynamic processes was carried out on a section of the Crimean coast adjacent to Lake Sasyk and including a transverse hydraulic structure.

Based on the analysis of the coastline position *in situ* measurements in the area of the structure for 2006–2014, it was found that the maximum range of interannual fluctuations was 5.8 m at the sections to the southeast of the structure and 3.4–7.2 m at the sections to the northwest. Seasonal variability is significantly higher: for example, their maximum range is 14.6 m at the sections southeastwards of the structure and 26.7 m at the sections to the northwest. Analysis of the coastline position satellite images in the structure area revealed that the range of coastline fluctuations is in very good agreement with the estimates obtained from *in situ* measurements.

The study of wave climate in the technological structure area was carried using the reanalysis data for 1979–2022. It indicated that the most probable direction of

wave approaching the coast is southwestern one with a frequency of > 30%. The highest waves also come from this direction. The extreme values of wave characteristics which can occur once in *n* years were obtained. The mean long-term values of storm numbers in the area under study are given depending on their duration.

Application of the *GenCade* integrated lithodynamic model permitted to obtain the estimates of changes in the coastline position in this area on the interannual scales. The model calculations made it possible to reproduce the main features and trends in changes of the beach width in the area of the structure obtained due to *in situ* observations. The mean annual sediment flows in the area under study are directed clockwise (to the southeast) that is conditioned by the coastline orientation and the wave climate features. Difference between the mean annual sediment rates at the area boundaries is negligible (< 4% of the multi-year average). This fact indicates insignificant impact of the structure upon the sediment total transfer to the southeast.

Under modern conditions, sediment flows in the area under study are balanced, and the coastline position is relatively stable. At the same time, cyclic changes in the coastline position directly at the water intake are typical. They are associated with changes in the directions of storm waves approaching the coast and, accordingly, the alongshore sediment flow. Any lithodynamic system consisting of both underwater (coastal slope) and above-water (beach) parts is extremely sensitive to the volumes and scales of external impacts. The construction of hydrodynamic structures in the coastal zone should be based on careful preliminary studies, including *in situ* observations, as well as physical and numerical modeling.

REFERENCES

1. Fomin, V.V. and Goryachkin, Yu.N., 2022. Accounting for the Local Wave and Morphodynamic Processes in Coastal Hydraulic Engineering. *Physical Oceanography*, 29(3), pp. 271-290. https://doi.org/10.22449/1573-160X-2022-3-271-290
2. Shuisky, Yu.D., 2005. Basical Peculiarities of Morphology and Dynamic of the Western Crimea Peninsula Coast. In: MHI, 2005. *Ecological Safety of Coastal and Shelf Zones and Comprehensive Use of Shelf Resources.* Sevastopol: ECOSI-Gidrofizika. Iss. 13, pp. 62-72 (in Russian).
3. Shuyskiy, Yu.D. and Karasyev, L.M., 1983. Eol Processes on Coastal Accumulative Forms in the West Crimea. Izvestiya VGO, 115(6), pp. 503-508 (in Russian).
4. Vykhovanets, G.V., 2003. [*Aeolian Process on the Sea Shore*]. Odessa: Astroprint, 368 p. (in Russian).
5. Goryachkin, Yu.N. and Dolotov, V.V., 2019. *Sea Coasts of Crimea*. Sevastopol: Kolorit Co. Ltd., 256 p. (in Russian).
6. Subetto, D.A., Sapelko, T.V., Stolba, V.F., Kuznetsov, D.D., Ludikova, A.V. and Neustrueva, I.Yu., 2023. Paleolimnology of Lakes of Western Crimea. *Doklady Earth Sciences*, 510(1), pp. 329-334. https://doi.org/10.1134/S1028334X23600184
7. Udovik, V.F. and Goryachkin, Yu.N., 2013. Interannual Variability of Alongshore Sediment Flux in the Coastal Zone of Western Crimea. In: MHI, 2013. *Ecological Safety of Coastal and Shelf Zones and Comprehensive Use of Shelf Resources*. Sevastopol: MHI. Iss. 27, pp. 363-368 (in Russian).
8. Divinsky, B.V., Fomin, V.V., Kosyan, R.D. and Ratner, Yu.D., 2020. Extreme Wind Waves in the Black Sea. *Oceanologia*, 62(1), pp. 23-30. https://doi.org/10.1016/j.oceano.2019.06.003
9. Amarouche, K. and Akpınar, A., 2021. Increasing Trend on Storm Wave Intensity in the Western Mediterranean. *Climate*, 9(1), 11. https://doi.org/10.3390/cli9010011

10. Leont'yev, I.O. and Akivis, T.M., 2020. The Effect of a Groin Field on a Sandy Beach. *Oceanology*, 60(3), pp. 412-420. https://doi.org/10.1134/S0001437020030042

11. Lazorenko, D.I., Kharitonova, L.V. and Fomin, V.V., 2016. Calculation of Changes Beach Shoreline Yevpatoriya Coast under the Influence Wind Waves. *Ecological Safety of Coastal and Shelf Zones of Sea*, (1), pp. 31-38 (in Russian).

12. Gurov, K.I., Udovik, V.F. and Fomin, V.V., 2019. Modeling of the Coastal Zone Relief and Granulometric Composition Changes of Sediments in the Region of the Bogaily Lake Bay-Bar (the Western Crimea) during Storm. *Physical Oceanography*, 26(2), pp. 170-180. https://doi.org/10.22449/1573-160X-2019-2-170-180

Submitted 12.12.2023; approved after review 06.05.2024;
accepted for publication 16.05.2024.

About the authors:

Yuri N. Goryachkin, Chief Research Associate, Marine Hydrophysical Institute of RAS (2 Kapitanskaya Str., Sevastopol, 299011, Russian Federation), DSc. (Geogr.), **ORCID ID: 0000-0002-2807-201X**, **ResearcherID: I-3062-2015**, yngor@mhi-ras.ru

Dmitry I. Lazorenko, Research Associate, Department of Computational Technologies and Mathematical Modeling, Marine Hydrophysical Institute of RAS (2 Kapitanskaya Str., Sevastopol, 299011, Russian Federation), CSc. (Tech.), **ORCID ID: 0000-0001-7524-565X**, **ResearcherID: J-1925-2015**, d.lazorenko.dntmm@gmail.com

Vladimir V. Fomin, Head of Department of Computational Technologies and Mathematical Modeling, Marine Hydrophysical Institute of RAS (2 Kapitanskaya Str., Sevastopol, 299011, Russian Federation), DSc. (Phys.-Math.), **ORCID ID: 0000-0002-9070-4460**, **ResearcherID: H-8185-2015**, v.fomin@mhi-ras.ru

Contribution of the co-authors:

Yuri N. Goryachkin – research initiation; formulation of the study goals and objectives; qualitative analysis of the results and their interpretation; discussion of the work results; formulation of conclusions; literature review on the research problem; search and critical analysis of materials in domestic and foreign sources; preparation of the paper text; editing and revision of the text; data visualization / presentation in the text

Dmitry I. Lazorenko – mathematical modeling of lithodynamic processes; analysis of modeling results; preparation of paper text; construction of tables, graphs, diagrams; discussion of paper materials; revision of paper text

Vladimir V. Fomin – mathematical modeling of wave regime; analysis of modeling results; preparation of paper text; construction of graphs, diagrams; discussion of the paper materials; revision of the paper text

The authors have read and approved the final manuscript.
The authors declare that they have no conflict of interest.